SUPPLEMENTARY INFORMATION FOR

Restrictive Eating Across A Spectrum from Healthy to Unhealthy –Behavioral and Neural Mechanisms

Karin Foerde, Janet E. Schebendach, Lauren Davis, Nathaniel Daw, B. Timothy Walsh, Daphna Shohamy, & Joanna E. Steinglass

SUPPLEMENTARY METHODS

Food Choice Task: Participants received a standardized lunch, consisting of 500 kcal (4 oz turkey breast, 2 slices whole wheat bread, 1 packet mayonnaise, Nutrigrain bar, and 8 oz water). The Food Choice Task with fMRI scanning occurred two hours later. The task consisted of three phases: Healthiness rating, Tastiness rating, and a Choice block (**Supplementary Figure 1**). Stimuli consisted of 76 images of food, half of which were classified as "high-fat" (>30% of the calories come from fat; images and macronutrient information available upon request).

In the rating phases, participants rated the food items for tastiness and healthiness on a 5-point Likert scale in two separate blocks. The rating scale appeared at the bottom of the screen for each item and participants were instructed that they could rate it as "neutral" or along the scale. For the Health block, the anchors were "Unhealthy" to "Healthy." For the Taste block, the anchors were "Bad" to "Good." For the Taste block, participants were additionally instructed to rate it *only* for tastiness. All task parameters (including order of the rating scale) were counterbalanced and randomized across participants. After completion of the rating scales, a "Reference" item was selected per individual participant that had been rated by them as "Neutral" on both tastiness and healthiness. Per published procedures (Foerde, Steinglass, Shohamy, & Walsh, 2015), if an individual did not identify an item as neutral on both scales, then an item was selected that was neutral on Health and 1 point in the positive direction on Taste. This method aims to minimize biasing choices based on taste value.

Figure S1. Food Choice Task. Healthiness rating phase (**A**), Tastiness rating phase (**B**), and Choice phase (**C**).

In the Choice block of the task, participants were instructed to identify on each trial whether they choose to eat the Reference item or the other trial-unique food item presented. The Reference item stayed the same throughout the Choice block and was presented on the left of the screen with a different food item per trial on the right side of the screen. On each trial, the participant

was instructed to select Strongly Prefer or Prefer for the Reference item or for the trial-unique item. Importantly, participants were instructed that they would be served one of their choices, selected at random, as a snack. At the end of the task, one choice block trial was randomly selected, and that afternoon the participant received a snack sized portion of their selected item on that trial, observed by staff. This procedure enhances confidence that the participant's responses reflect true preferences.

In all blocks, the food stimulus was presented for 4 seconds on each trial, during which participants made their response. Each trial was followed by a fixation cross inter-trial interval (ITI). The duration of ITIs was jittered for optimization of event-related fMRI design. Stimulus presentation sequence and timing were optimized using the optseq2 algorithm (http://surfer.nmr.mgh. harvard.edu/optseq/). Each learning run lasted 480 s. Mean ITI = 2.3 s, median = 2 s, and range = 1–10 s, across all three phases. All task phases were presented using Matlab and the Psychophysics toolbox (Brainard, 1997).

Detailed Imaging Procedures

Image Pre-processing: Imaging data were converted from DICOM to NIFTI format and preprocessed and analyzed using the FSL (http://fsl.fmrib. ox.ac.uk/fsl/) package version 6 (FMRIB's Software Library; Oxford Centre for Functional Resonance Imaging of the Brain, FMRIB)(Smith et al., 2004). Functional images were aligned using the MCFLIRT tool (Jenkinson, Bannister, Brady, & Smith, 2002) and the six scan-to-scan head motion parameters estimated during motion correction obtained. The skull was removed from functional images using the brain extraction tool (BET) (Smith, 2002) and from structural images using Freesurfer (Fischl, Sereno, Tootell, & Dale, 1999; Segonne et al., 2004). Spatial smoothing was applied with a Gaussian kernel of 5 mm (FWHM). Data and design matrix were high-pass filtered with a cutoff period of 100 s. After analysis at the individual level, the results were normalized to a standard template. The following steps were performed to improve registration and obviate concerns about potential brain atrophy in individuals with AN due to malnutrition: Functional images were first aligned to the T1-weighted image using a boundary-based registration method implemented in FSL6 (BBR) and then the structural image to the standard MNI152 2-mm template using FLIRT (12 degrees of freedom) and FNIRT (10-mm warp resolution) (Andersson, Jenkinson, & Smith, 2007; Jenkinson et al., 2002).

Supplementary Data Analyses

fMRI Analyses of sample matched behaviorally to previous sample (Foerde et al., 2015)

To test whether the neural group difference between HC and AN observed in our prior study replicated in the current independent sample, we performed a set of secondary analyses. In order to more directly compare the samples, because of study differences, we constrained our sample to include participants whose high-fat food choice behavior was within the distribution of our prior study. Participants in the current HC group included those whose high-fat food choices were above the minimum in the HC group in the prior study (i.e., the 1st quartile–1.5 x interquartile range; IQR). Participants in current AN group included those whose high-fat food choices fell below the maximum for the AN group in the prior study (i.e., the 3rd quartile+1.5 x IQR). The resulting sample included 29 HC and 24 AN.

Caudate-VMPFC functional connectivity analysis.

To assess functional connectivity between our caudate and VMPFC ROIs we estimated a psychophysiological interaction (PPI) model in the Choice phase following the approach outlined in FSL's Feat module (http://fsl.fmrib.ox.ac.uk/fsl/fslwiki/PPIHowToRun). We used the right anterior caudate ROI as the seed region (Supplementary **Fig. S7**). Masks created in standard space were transformed into each participant's functional native space and time-courses extracted for each participant. The model included a psychological regressor comparing high- versus low- fat foods (coded as 1 and –1, respectively) convolved with an HRF, a physiological regressor (the time course extracted from the seed region), the interaction between the two (the regressor of interest), a regressor with onsets for high- plus low-fat trials, and a regressor for missed trials. In addition, motion and confound regressors were included as for other analyses. Connectivity differences between groups were assessed by extracting data from the VMPFC ROI (Main text, **Fig. 4**) and comparing groups using t-tests.

SUPPLEMENTARY RESULTS

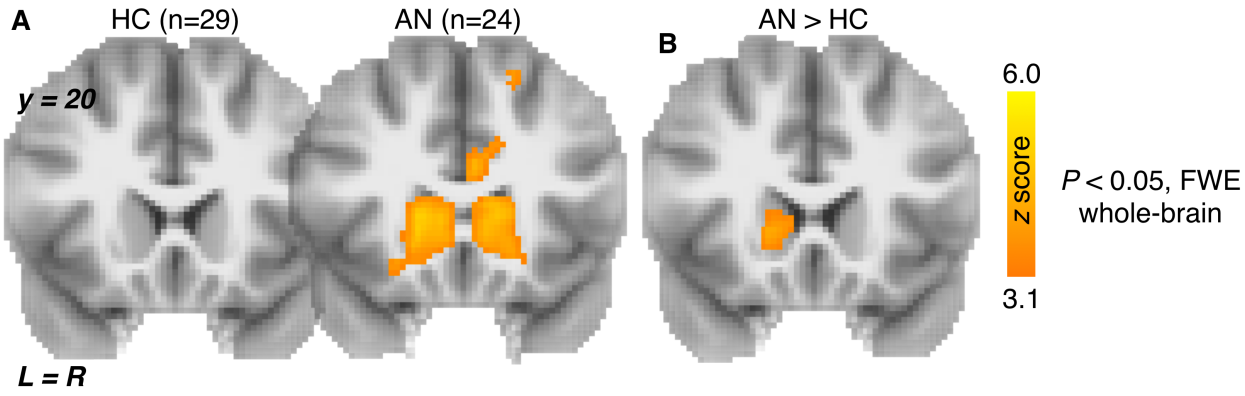

Figure S2. Neural systems engaged during food choice across subsampled HC and AN participants. (**A**) Regions correlated with choice values in a parametric analysis in HC (left) and AN (right) groups subsampled to behaviorally match participants in a previous study using the Food choice task (Foerde et al., 2015). HC participants from the current sample whose high-fat food choices were above the "minimum" box-plot range (i.e., the 1st quartile–1.5 IQR) of the previous study were sampled, and AN participants from the current sample whose high-fat food choices were below the "maximum" box-plot range (i.e., the 3rd quartile+1.5) of our previous study were sampled. Whole-brain family-wise error (FWE)-corrected $p<0.05$, cluster-forming threshold $Z > 3.1$. (**B**) Direct comparison of subsampled HC and AN groups showed significantly greater activity in the caudate among AN than HC (whole-brain FWE-corrected $p<0.05$, cluster-forming threshold $Z>3.1$).

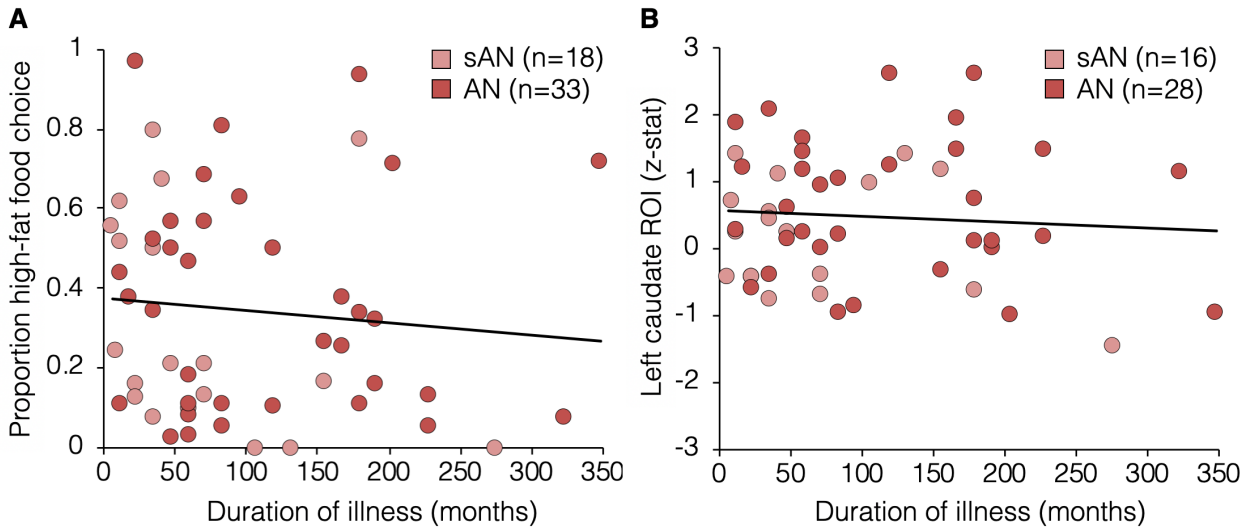

Figure S3. Correlations with Duration of Illness. (**A**) There was no significant association between duration of illness and proportion choices of high-fat foods on the Food Choice Task (r=-0.094, p=498). (**B**) Choice-related activation of the caudate was not significantly associated with duration of illness (r=-0.077, p=0.59).

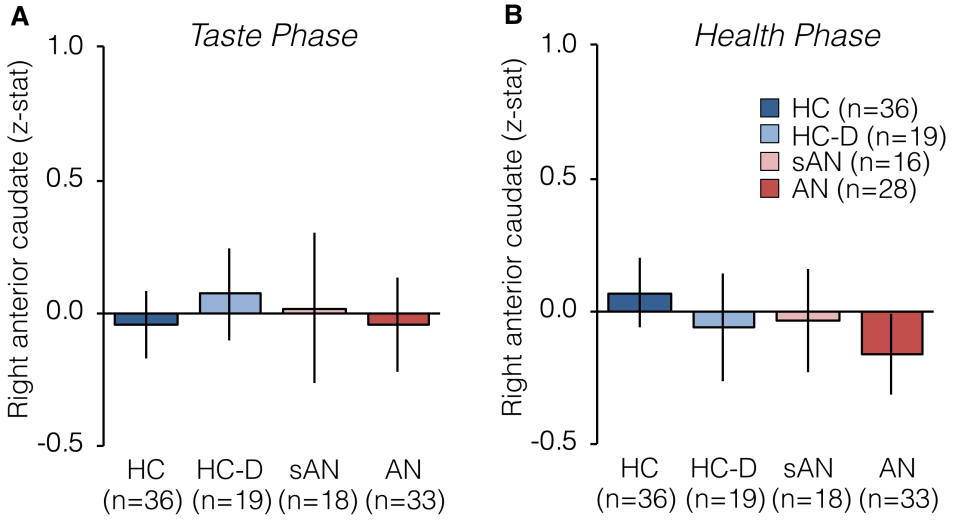

Figure S4. Rating phase caudate ROI analyses. We assessed right anterior caudate responses (same region assessed for the Choice phase) in the Health and Taste rating phases. Groups did not differ in Taste (**A**) or Health (**B**) rating phases.

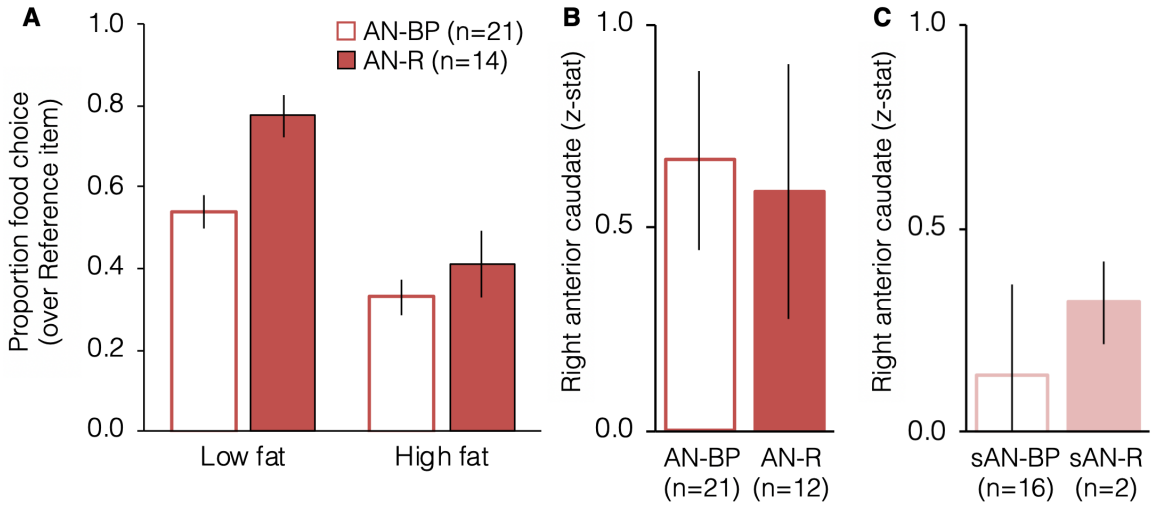

Figure S5. Food choices in AN restricting and binge-eating/purging subtypes. (**A**) Restricting (AN-R) and binge-eating/purging (AN-BP) subtypes of AN were not evenly distributed (40% restricting), and the study was not designed to assess differences between these subtypes. In the laboratory multi-item meal, there were no significant differences between AN-R and AN-BP subtypes (t_{26}=-0.97, p=0.34). Exploratory analyses comparing food choices of AN subtypes in a mixed ANOVA found a main effect of Food Type, with fewer choices of high-fat than low-fat foods (F(1,33) = 41.38, p< 0.001), and a main effect of Subtype, such that the individuals with AN-BP subtype were less likely to choose the trial-unique food items overall (F(1,33) = 5.70, p = 0.023), but no interaction between Food Type and Subtype (F(1,33) = 3.06, p = 0.09). Independent samples T-tests showed no significant subtype differences on high-fat food trials (t(33) = -0.85, p =0.4), only on low-fat food trials (t(33)=-3.81, p < 0.001). Forty percent of individuals with AN-R subtype and 24 percent of those with AN-BP subtype had a Reference food item from the high-fat category; these proportions were not significantly different (X^2(1) = 1.41, p = 0.23). (**B**) Activity in the caudate ROI for individuals with AN-BP and AN-R subtypes is presented for illustration purposes (statistical comparison was not undertaken due to the small sample sizes). (**C**) In addition, activity in the caudate ROI is shown for restricting and binge-eating/purging subtypes for the sAN group. Statistical comparison was not undertaken due to the small sample sizes and note that only two individuals in the sAN group were of the restricting subtype.

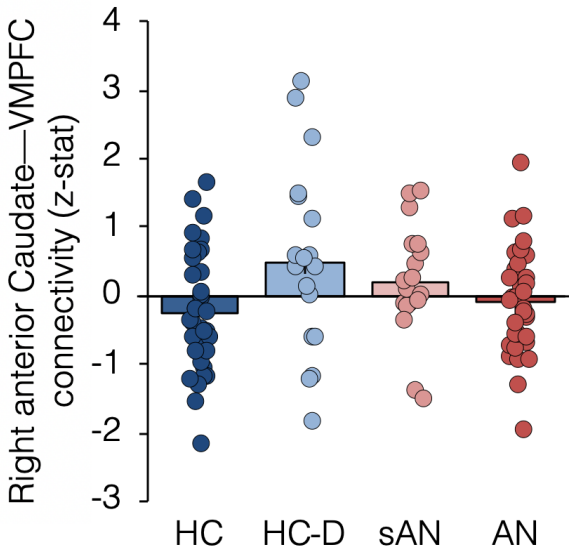

Figure S6. Comparison of Caudate-VMPFC functional connectivity across groups. Values extracted from the functional connectivity analysis in the choice phase from our a priori anatomical ROI in the VMPFC (see Figure 4). Individual subjects are overlaid on bars representing the means for each group. The HC-D group differed from the HC (t_{53}=-2.61, p=0.012) and AN group (t_{50}=-2.12, p=0.039) and no other pairwise differences were significant (ps > 0.05). The HC-D groups included two extreme values; without those participants, differences between HC-D and HC (t_{51}=-1.77, p=0.083) and AN (t_{48}=-1.24, p=0.221) were no longer significant.

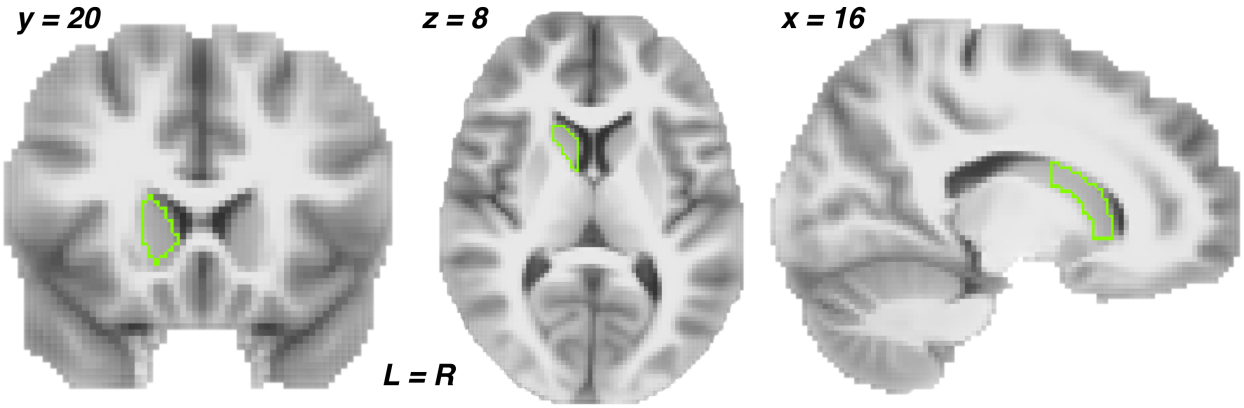

Figure S7. Region of interest. Anatomical ROI in anterior, right, caudate outlined in green.

Supplementary Table S1. Food Choice Task Reference food ratings across groups.

		Healthiness rating						Tastiness rating					
Group	n	1	2	3	4	5	None	1	2	3	4	5	None
HC	36	0	0	36	0	0	0	0	0	33	3	0	0
AN	35	0	0	33	2	0	0	0	0	34	1	0	0
sAN	19	0	0	19	0	0	0	0	0	18	1	0	0
HC-D	20	1	1	17	1	0	0	0	0	19	0	0	1*
Total	110	1	1	105	3	0	0	0	0	104	5	0	1

* One HC-D used only extreme ratings (1 and 5) and was given the default reference item of "saltines" for which no response had been made in the Taste block.

Supplementary Table S2. Results from the whole-brain parametric analysis of choice ratings (FWE-corrected, z=3.1, $p < 0.05$).

	Cluster	Left/ Right	Region	Cluster size	x	y	z	Peak Z
HC	1	L	Paracing. gyrus /Frontal Medial Ctx	1425	-4	52	-4	5.19
		L	Paracing. gyrus		-6	44	0	5.01
		R	Paracing. gyrus		6	52	-4	4.63
		L	Ant cingulate		-6	44	8	4.63
			Paracing. gyrus/Frontal Medial Ctx		0	56	8	4.34
		R	Paracing. gyrus /Frontal Medial Ctx		10	44	-6	4.24
	2	R	Intracalcarine	859	12	-88	0	5.18
		R	Lingual Gyrus		16	-80	-2	4.75
		R	Fusiform gyrus		34	-74	-16	4.22
		R	Fusiform gyrus		28	-76	-10	4.14
		R	Fusiform gyrus		30	-76	-16	4.05
		R	Lateral Occipital Ctx		36	-70	-4	3.25
	3	L	Superior Frontal gyrus	229	-20	22	42	3.8
		L	Superior Frontal gyrus		-18	26	40	3.78
		L	Superior Frontal gyrus		-18	36	40	3.57
		L	Superior Frontal gyrus		-18	34	46	3.56
		L	Superior Frontal gyrus		-18	42	46	3.52
		L	Superior Frontal gyrus		-24	28	50	3.29
	4	L	Precuneus	160	-6	-54	14	3.96
AN	1	R	Occipital Fusiform Gyrus	3644	26	-78	-12	5.83
		R	Intracalcarine		14	-86	2	5.77
		R	Fusiform gyrus		16	-78	-18	5.59
		R	Intracalcarine		14	-76	-4	5.49
		R	Lingual Gyrus		10	-72	-12	5.45
		R	Lateral Occipital Ctx		26	-88	22	5.35
	2		Frontal Pole/Medial Frontal Gyrus	2498	0	58	8	5.18
		L	Paracingulate Gyrus		-12	50	-2	4.98
		L	Frontal Pole/Medial Frontal Gyrus		-4	56	-2	4.87
		L	Paracingulate Gyrus		-10	38	20	4.84
		L	Orbitofrontal Ctx		-24	44	-12	4.8
		L	Paracingulate Gyrus		-8	46	-8	4.69
	3	L	Caudate	1310	-8	22	-2	4.99
		L	Caudate		-16	22	8	4.8
		R	Caudate		16	24	2	4.76
		L	Nucleus Accumbens		-14	16	-6	4.44
		L	Caudate		-14	18	-2	4.43
		R	Caudate		8	22	0	4.36
	4	L	Precuneus	543	-4	-58	18	4.5
		L	Precuneus		-10	-54	22	4.24

		L	Precuneus		-2	-58	6	4.2
		L	Precuneus		-10	-56	12	3.83
		L	Posterior Cingulate		-4	-50	10	3.68
		L	Cuneal Ctx/Precuneus		-6	-72	22	3.42
	5	L	Superior Frontal Gyrus	275	-20	26	62	4.07
		L	Superior Frontal Gyrus		-18	38	48	3.9
		L	Superior Frontal Gyrus		-22	34	50	3.84
		L	Superior Frontal Gyrus		-18	22	56	3.82
		L	Frontal Pole		-18	44	44	3.56
		L	Superior Frontal Gyrus		-22	30	58	3.54
	6	L	Postcentral Gyrus	229	-46	-30	58	4.45
	7	L	Precuneus	170	-4	-44	46	3.84
		L	Posterior Cingulate		-6	-36	38	3.83
		R	Posterior Cingulate		2	-30	40	3.57
		L	Posterior Cingulate		-4	-28	34	3.33
		L	Posterior Cingulate		-2	-32	48	3.23
		L	Precentral Gyrus		-6	-30	48	3.21
HCD	1	R	Ant Cingulate/Frontal Medial Ctx	210	4	34	10	3.98
		R	Ant Cingulate/Frontal Medial Ctx		4	42	4	3.93
		R	Ant Cingulate/Frontal Medial Ctx		8	40	-2	3.88
		R	Paracingulate gyrus		8	44	-6	3.63
		L	Paracingulate gyrus		-6	44	2	3.49
			Paracingulate gyrus		0	46	-2	3.43
sAN*	No significant clusters FWE-corrected, z=3.1, p<0.05; FWE-corrected, z=2.3, p<0.05 shown below							
	1	R	Lingual gyrus	979	12	-80	-6	3.79
		R	Fusiform gyrus		24	-72	-4	3.46
		R	Lingual gyrus		12	-84	2	3.37
		R	Fusiform gyrus		16	-80	-16	2.95
		R	Lateral Occipital cortex		34	-88	-4	2.94
		R	Lateral Occipital cortex		40	-82	0	2.68
	2	L	Paracingulate Gyrus	693	-6	32	30	3.51
		L	Paracingulate Gyrus		-2	36	32	3.46
		L	Anterior cingulate		-8	30	24	3.4
		L	Paracingulate Gyrus		-2	34	24	3.31
		R	Paracingulate Gyrus		2	38	26	3.18
		R	Paracingulate Gyrus		10	34	26	3.06
	3	L	Middle frontal gyrus	613	-34	30	32	3.54
		L	Frontal pole		-22	46	30	3.3
		L	Superior Frontal Gyrus		-18	30	48	3.04
		L	Superior Frontal Gyrus		-22	34	36	3.02

For each cluster, the peak and 5 local maxima within the cluster are listed along with x-y-z locations in MNI space.

No pair-wise group differences survived correction at FWE-corrected, $z=3.1$, $p < 0.05$.

SUPPLEMENTARY REFERENCES

Andersson, J. L., Jenkinson, M., & Smith, S. (2007). *Non-linear registration aka Spatial normalisation FMRIB Technial Report TR07JA2*. FMRIB Analysis Group of the University of Oxford.

Brainard, D. H. (1997). The Psychophysics Toolbox. *Spatial Vision, 10*(4), 433-436.

Fischl, B., Sereno, M. I., Tootell, R. B., & Dale, A. M. (1999). High-resolution intersubject averaging and a coordinate system for the cortical surface. *Human Brain Mapping, 8*(4), 272-284.

Foerde, K., Steinglass, J. E., Shohamy, D., & Walsh, B. T. (2015). Neural mechanisms supporting maladaptive food choices in anorexia nervosa. *Nature Neuroscience, 18*(11), 1571-1573.

Jenkinson, M., Bannister, P., Brady, M., & Smith, S. (2002). Improved optimization for the robust and accurate linear registration and motion correction of brain images. *Neuroimage, 17*(2), 825-841.

Segonne, F., Dale, A. M., Busa, E., Glessner, M., Salat, D., Hahn, H. K., & Fischl, B. (2004). A hybrid approach to the skull stripping problem in MRI. *Neuroimage, 22*(3), 1060-1075.

Smith, S. M. (2002). Fast robust automated brain extraction. *Human Brain Mapping, 17*(3), 143-155.

Smith, S. M., Jenkinson, M., Woolrich, M. W., Beckmann, C. F., Behrens, T. E., Johansen-Berg, H., . . . Matthews, P. M. (2004). Advances in functional and structural MR image analysis and implementation as FSL. *Neuroimage, 23 Suppl 1*, S208-219.